

Oxide templates for self-assembling arrays of metal nanoclusters

N. Berdunov^{a,*}, G. Mariotto^b, K. Balakrishnan^b, S. Murphy^b, I.V. Shvets^b

^a School of Physics and Astronomy, Nottingham University NG7 2RD, UK

^b Centre for Research on Adaptive Nanostructures and Nanodevices, Physics Department, Trinity College, Dublin 2, Ireland

Received 31 May 2006; accepted for publication 28 July 2006

Available online 28 August 2006

Abstract

We demonstrate that ordered arrays of metal clusters of a few nanometers in size can be fabricated by self-assembly on a range of oxide nanotemplates. Two systems were chosen, FeO/Pt(111) and Fe₃O₄, having in common a reconstructed close-packed oxygen surface layer. Deposition of various metal films results in the formation of nanosized clusters arranged according to the surface long-range order. Employing ab-initio calculations we discuss the observed mechanism of site-selective nucleation of the metal nanoclusters. Finally, we discuss the existence of a wide family oxide templates that can be used for self-assembled growth of nanoclusters governed by the same rules.

© 2006 Elsevier B.V. All rights reserved.

Keywords: Self-assembly of nanocluster arrays; Patterned oxide surfaces; Nanotemplates

Nanometer scale structures, like nanodots, wires, crystals, etc. have recently attracted a lot of interest because of their potential for use in novel device applications for magnetic recording, sensors, quantum computing, short-wavelength optics and spin electronics. For example, the magnetic anisotropy of nanostructured media can be tailored by simply changing the shape and size of the nanostructures it comprises, which can be used for new magnetic storage media [1]. Electron confinement in such nano-objects would also facilitate quantum-computing applications. Achieving periodic ordering within a particulate media would provide coherent superposition of spin-electron states at the nanometer scale, which is essential for spin-transport applications [2]. To realise a device based on such nano-objects it is essential to have a large number of identical nano-objects acting in the same manner, i.e. representing a collective behavior [3]. Thus, an array of crystallites regularly arranged and of uniform size/orientation is a desirable medium. We present two examples of oxide nanotemplates for self-assembled epitax-

ial growth of nanocluster arrays [4–9], which demonstrate the possibility of tuning the size and spatial order of metal clusters. The following templates were investigated: FeO/Pt(111) and Fe₃O₄(111). All experiments were performed in UHV conditions at a base pressure of 2×10^{-10} Torr. Metal ultrathin films were deposited by e-beam evaporation at room temperature using a quartz crystal balance monitor for thickness control. LEED and STM measurements were used to monitor the film quality. Constant current STM scans were performed at room temperature.

1. Oxygen-terminated Fe₃O₄(111) nanotemplate

In this experiment, a Fe₃O₄(111) single crystal and a 100 nm Fe₃O₄(111) film grown on MgO(111) were used (for growth conditions see [10]). Both Fe₃O₄ substrates were oxidised in 10^{-6} Torr O₂ at 1000 K [11]. In the case of the Fe₃O₄/MgO film, the annealing time was only 2 min, to prevent significant diffusion of Mg to the surface. This results in a 4.2 nm superstructure covering almost the entire sample surface. As we have shown in our previous work [11] this represents an oxygen-terminated surface, which reconstructs under intrinsic stress creating a long-range order.

* Corresponding author.

E-mail address: nikolai.berdunov@nottingham.ac.uk (N. Berdunov).

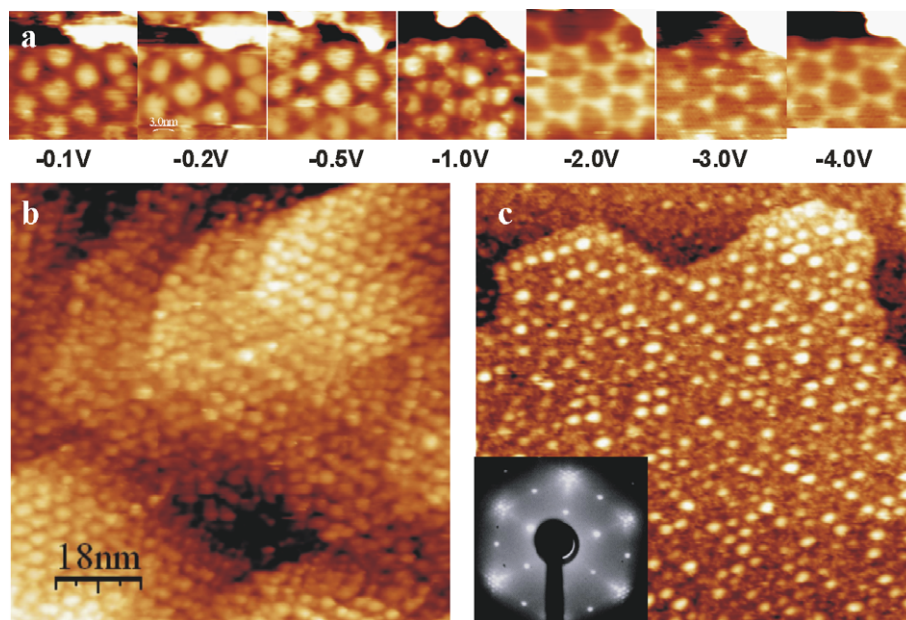


Fig. 1. (a) Series of STM images of $\text{Fe}_3\text{O}_4(111)$ superstructured surface taken at different tunneling bias showing the inversion of tunneling contrast; (b) STM images of 2 Å Fe film deposited on 100 nm film $\text{Fe}_3\text{O}_4/\text{MgO}(111)$ and (c) 0.5 Å Cr-film deposited on single crystal $\text{Fe}_3\text{O}_4(111)$. Initially, both samples were annealed in oxygen atmosphere to form an oxygen-terminated surface reconstructed into a 4.2 nm superstructure. Clusters of 2 AL (b) and 1 AL (c) thickness form an ordered array with the superstructure periodicity; (inset-c shows a LEED picture of the surface after deposition).

The long-range order reveals a charge modulation along the surface seen in bias-dependent STM images (Fig. 1(a)). As it has been found in [12], this surface charge redistribution is due to surface strain governing the interaction between oxygen and iron. Thus the effective surface oxygen charge changes following the surface strain pattern. One can therefore expect significant variations in adsorption properties across the surface superstructure.

Deposition of Fe and Cr films results in the formation of regular arrays of nanoclusters on the magnetite surface Fig. 1(b), (c). In the case of 0.5 Å and 1 Å film thickness, the clusters' height is one atomic layer (AL) [13], whereas a 2 Å thick film results in 2 AL clusters formation, conserving the arrays regularity. LEED measurements (Fig. 1(c) inset) suggest that the Fe and Cr clusters grow epitaxially as a sharp LEED pattern is obtained.

2. FeO/Pt(111) nanotemplate

The growth of a single FeO layer on Pt(111) results in a coincidence structure (Moiré pattern) of 2.6 nm periodicity [14]. The FeO film was formed by depositing 1 Å of Fe on a Pt(111) substrate and post oxidising it in 10^{-6} Torr O_2 at 1000 K for 2 min similar to [14]. Fig. 2(a) shows Fe clusters nucleated on the surface after depositing 0.2 Å Fe film. The clusters are well confined and repeat the surface superlattice. LEED patterns taken before and after deposition (Fig. 2(c)) confirm that low iron coverage does not destroy FeO/Pt(111) superstructure.

The 'site selective' nucleation is demonstrated in Fig. 2(b) corresponding to 0.05 Å of vanadium deposited on the superstructured FeO/Pt(111) surface. In the STM

image it is possible to identify the vanadium clusters' nucleation sites. According to the FeO/Pt(111) model Fig. 2(d) and STM simulations [14,15] the hcp sites appear as bright protrusions (Fig. 3(b)), when the vanadium clusters are positioned where the FeO layer forms fcc stacking sequence with the platinum surface, i.e. the darker regions between the hcp sites.

We have performed DFT calculations to identify the geometry of a single atomic layer of adsorbed metal film. The CASTEP program [16] as a module of Materials Studio has been used in all our Density Functional Theory (DFT) calculations. The local density GGA functional with ultrasoft pseudopotentials was used to optimize the surface geometry, calculate the electron density distribution and adsorption energy. A single unit cell vacuum slab of FeO/Pt(111) similar to that used in [7] and a second with the FeO film shifted to form an hcp stacking sequence with the substrate have been used for adsorption energy calculations. A plane wave cutoff of 340 eV and a $(6 \times 6 \times 1)$ grid of k -points were chosen. The calculation results suggest that in both cases the favourable adsorption sites for Fe adatoms are on-top of oxygen. The calculated interlayer distance of 1.8 Å between adsorbed Fe and surface oxygen is well in agreement with STM measured values of 1.5–1.8 Å. Surprisingly, the difference in the adsorption energy between fcc and hcp FeO/Pt(111) configuration is only about 0.1 eV, which suggests that there is probably another mechanism involved in the preferential nucleation observed in the experiments.

In the cases presented above, the reason for the long-range surface reconstruction is a structural instability: either due to a non-uniform oxygen lattice as in magnetite

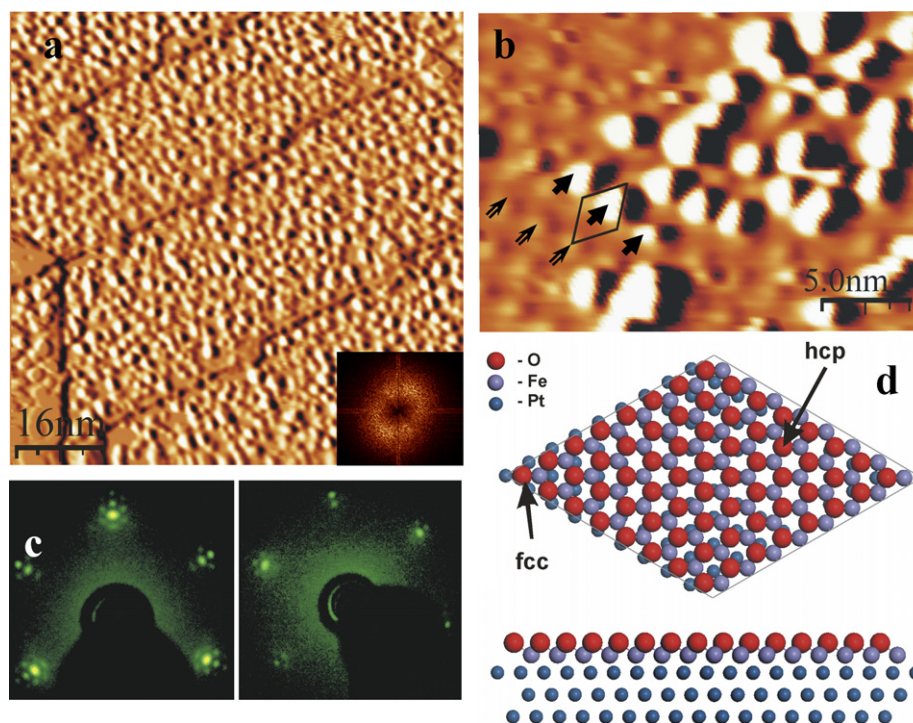


Fig. 2. (a) STM image of 0.2 Å Fe film grown on FeO/Pt(111) template. Clusters of 1 AL thickness nucleate following the long-range surface superstructure of 2.6 nm periodicity. The image is presented in differentiated contrast. 2D Fourier transformation image shows preferred clusters' periodicity of 2.6 ± 0.6 nm. (b) Demonstration of 'site selective' nucleation of vanadium clusters (white spots) after depositing a 0.05 Å vanadium film. The smaller corrugation seen on the image is the surface superstructure. Three hollow arrows point out the hcp sites of FeO/Pt(111) and the solid arrows indicate the vanadium clusters nucleated at fcc sites. Unit cell of FeO/Pt(111) superstructure is indicated. (c) LEED pictures before (left) and after (right) depositing a 0.2 Å Fe film. (d) The model of FeO/Pt(111) coincidence structure [13], comprising a FeO bi-layer on the Pt(111) surface (top-view and side-view). Two sites of FeO forming an fcc and an hcp stacking sequence with Pt(111) surface are indicated.

[11], or caused by a film's mismatch with the substrate and surface polarity [17]. In some cases, the distortion in the oxygen lattice is evident from STM data [7,11,15], while in others the existence of the strain in the surface layer can be deduced from the local variations in the stacking sequence. In particular, fcc and hcp local structures, which can be identified in the FeO/Pt(111) coincidence structure (Fig. 2(b)), relax differently resulting in a lateral strain modulation. Thus, geometry optimization of the single FeO layer on Pt(111) gives us two stable structures with different in-plane lattice constants of 3.1 Å and 2.8 Å. The first value is for FeO single layer relaxed on a fcc site and the second on an hcp site Fig. 2(b).

To understand the effect of the strain/distortion in the top surface layer we have performed DFT calculations for the FeO(111) laterally distorted structure.¹ The calculated values of adsorption energy for the Fe adlayer gives 1 eV stronger adsorption in the case of stretched FeO (3.1 Å), which is much stronger than the 0.1 eV adsorption energy difference between fcc and hcp FeO/Pt(111). This suggests that the local distortion has a greater effect on

binding energy than stacking sequence variations. Fig. 3 shows that charge transfer between the surface oxygen and the iron in the layer below depends on the lateral stress [12,18]. This also explains surface charge modulation across the surface superstructure observed in our bias-dependent STM images Fig. 1(a) and also in Ref. [19]. Therefore, we conclude that the lateral charge re-allocation caused by the Fe–O bond distortion results in a modulation of the surface binding energy within the surface superlattice, which gives rise to the preferential nucleation of the metal clusters. Moreover, in contrast to the easy oxidized metals used in our experiments, gold clusters preferential nucleation can only be observed at low temperature due to lesser adhesion as has been demonstrated in [19].

A close-packed oxygen termination is a common feature of type three polar surfaces for (111) and (0001) orientations of oxide crystals [17], so the other oxides of this family may display similar reconstructions. Among the experimental reports on long-range reconstructions of oxygen-terminated oxide surfaces we have identified a number of systems which fall into our nanotemplate family [8,11,14,15,20–29]. Thus, FeO grown on Rh(111) [15] forms a coincidence structure similar to FeO/Pt(111) but smaller periodicity of 1.4 nm due to the large film/substrate mismatch. In some cases, growth of a native oxide by oxidizing a metal substrate results in the formation of similar

¹ DFT calculations settings: GGA-PBE functional, $8 \times 8 \times 1$ k -point set, 300 eV energy cutoff; two vacuum slabs constructed of 7 Å thick FeO with in-plane lattice constants of (2.8 Å × 2.8 Å) and (3.1 Å × 3.1 Å) and 10 Å of vacuum; full geometry optimization performed for fixed unit cell.

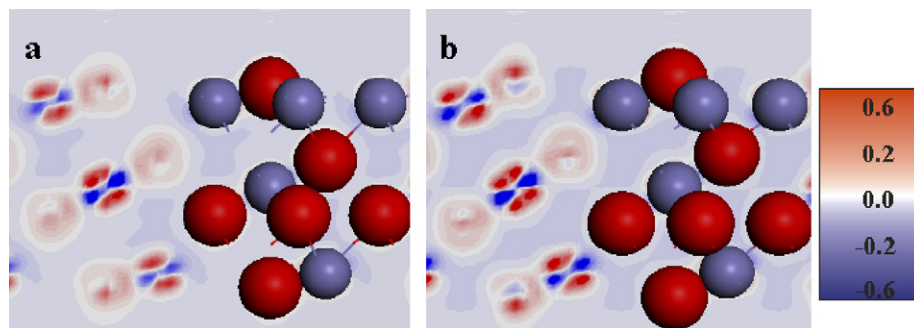


Fig. 3. Cross-sectional view of the FeO vacuum slab and charge density difference distribution for stretched (a) and compressed (b) FeO, corresponding to in-plane lattice constants of 3.1 Å and 2.8 Å, respectively.

surface superstructure as been demonstrated in the case of RhO₂/Rh(111) and been exploited to form Fe-clusters arrays [15]. In all these examples the superstructure periodicity ranges from 1.4 nm to 4.5 nm. The future expansion of this list will give us the freedom of tailoring the nanoclusters in size and array spacing. Moreover, the different spin/electron transport properties of the substrates provide enormous potential for manufacturing high-performance magnetic and spin-transport materials and also for molecular engineering.

Acknowledgement

This work was supported by CRANN and Science Foundation of Ireland (SFI) under contract 00/PI.1/C042.

References

- [1] R. Skomski, *J. Phys.: Condens. Matter* 15 (2003) R841.
- [2] I. Zutic, J. Fabian, S. Das Sarma, *Rev. Mod. Physics* 76 (2004) 323; C.T. Black, C.B. Murray, R.L. Sandstrom, S.H. Sun, *Science* 290 (2000) 1131.
- [3] A. Courty, A. Mermet, P.A. Albouy, E. Duval, M.P. Pileni, *Nature Mat.* 4 (2005) 395.
- [4] H. Brune, M. Giovannini, K. Bromann, K. Kern, *Nature* 394 (1998) 451.
- [5] V. Repain, J.M. Berroir, S. Rousset, J. Lecoer, *Surf. Sci.* 447 (2000) L152.
- [6] M.H. Pan, H. Liu, J.Z. Wang, J.F. Jia, Q.K. Xue, J.L. Li, S. Qin, U.M. Mirsaidov, X.R. Wang, J.T. Markert, Z.Y. Zhang, C.K. Shih, *Nano Lett.* 5 (2005) 87.
- [7] S.K. Shaikhutdinov, R. Meyer, D. Lahav, M. Baumer, T. Kluner, H.J. Freund, *PRL* 91 (2003) 076102.
- [8] S. Degen, C. Becker, K. Wandelt, *Faraday Discussions* 125 (2004) 343.
- [9] W.-C. Lin, C.-C. Kuo, M.-F. Luo, K.-J. Song, M.-T. Lin, *APL* 86 (2005) 043105.
- [10] K. Balakrishnan, S.K. Arora, I.V. Shvets, *J. Phys. Condens. Matter* 16 (2004) 5387.
- [11] N. Berdunov, S. Murphy, G. Mariotto, I.V. Shvets, *PRB* 70 (2004) 085404.
- [12] N. Berdunov, S. Murphy, G. Mariotto, I.V. Shvets, *PRL* 93 (2004) 057201.
- [13] N. Berdunov, G. Mariotto, S. Murphy, K. Balakrishnan, I.V. Shvets, *PRB* 71 (2005) 113406.
- [14] H.C. Galloway, P. Sautet, M. Salmeron, *PRB* 54 (1996) R11145.
- [15] N. Berdunov, G. Mariotto, I.V. Shvets, to be published, see also http://www.nottingham.ac.uk/~ppznb/FeO_on_Rh.html; <http://www.nottingham.ac.uk/~ppznb/others.html>.
- [16] M.D. Segall, P.J.D. Lindan, M.J. Probert, C.J. Pickard, P.J. Hasnip, S.J. Clark, M.C. Payne, *J. Phys. Condens. Matter* 14 (2002) 2717.
- [17] C. Noguera, *J. Phys.: Condens. Matter* 12 (2000) R367.
- [18] M. Todorova, K. Reuter, M. Scheffler, *PRB* 71 (2005) 195403.
- [19] E.D.L. Rienks, N. Nilius, H.-P. Rust, H.-J. Freund, *PRB* 71 (2005) 241404; N. Nilius, E.D.L. Rienks, H.-P. Rust, H.-J. Freund, *PRL* 95 (2005) 066101.
- [20] N.G. Condon, F.M. Leibsle, T. Parker, A.R. Lennie, D.J. Vaughan, G. Thornton, *PRB* 55 (1997) 15885.
- [21] N.G. Condon, F.M. Leibsle, A.R. Lennie, P.W. Murray, D.J. Vaughan, G. Thornton, *PRL* 75 (1995) 1961.
- [22] C. Barth, M. Reichling, *Nature* 414 (2001) 54.
- [23] R.A. Fellows, A.R. Lennie, A.W. Munz, D.J. Vaughan, G. Thornton, *American Mineralogist* 84 (1999) 1384.
- [24] J. Schoiswohl, M. Sock, S. Esk, S. Surnev, M.G. Ramsey, F.P. Netzer, G. Kresse, *PRB* 69 (2004) 155403.
- [25] G. Ketteler, W. Ranke, *PRB* 66 (2002) 033405.
- [26] A. Mannig, Z. Zhao, D. Rosenthal, K. Christmann, H. Hoster, H. Rauscher, R.J. Behm, *Surf. Sci.* 576 (2005) 29.
- [27] F. Sedona, G.A. Rizzi, S. Agnoli, F.X. Llabrés i Xamena, A. Papageorgiou, D. Ostermann, M. Sambri, P. Finetti, K. Schierbaum, G. Granozzi, *J. Phys. Chem. B* 109 (2005) 24411.
- [28] J.V. Barth, G. Costantini, K. Kern, *Nature* 437 (2005) 671.
- [29] J. Gustafson, A. Mikkelsen, M. Borg, E. Lundgren, L. Kohler, G. Kresse, M. Schmid, P. Vagra, J. Yuhara, X. Torrelles, C. Quiros, J.N. Andersen, *PRL* 92 (2004) 126102.